Electron paramagnetic resonance study of the Ce^{3+} pair centers in $YAlO_3$:Ce scintillator crystals

M. Buryi,[1] V. V. Laguta,[1,2] E. Mihóková,[1] P. Novák,[1] and M. Nikl[1]
[1]*Institute of Physics AS CR, Cukrovarnicka 10, Prague, 16200, Czech Republic*
[2]*Institute of Physics, Opole University, Oleska 48, 45-052 Opole, Poland*
(Received 22 July 2015; revised manuscript received 2 October 2015; published 9 December 2015)

Single crystals of $YAlO_3$ doped with Ce have been studied by electron paramagnetic resonance (EPR) at the 9.4 and 34 GHz microwave bands. Besides the single-ion Ce^{3+} spectrum, measurements have revealed many satellite lines which belong to the Ce^{3+}-Ce^{3+} pair centers. Their spectra have been fitted by a general effective spin Hamiltonian describing two interacting particles with the spin $S = 1/2$. Corresponding g factors and spin-spin coupling constants have been determined. The spin-spin coupling constants are in the range from 0.1 up to 0.65 cm^{-1} for the nearest and next-nearest neighbors depending on the distance between Ce ions and their position. The exchange interaction between next-nearest neighbors (NNNs) is comparable to or even bigger than that between nearest neighbors (NNs), being in the range $0.4 - 0.6\,cm^{-1}$. For a single Ce^{3+} ion, crystal field parameters, energy sublevels of the $^2F_{5/2}$ and $^2F_{7/2}$ multiplets and principal g tensor components were obtained from the density functional theory calculation. They are in satisfactory agreement with those determined experimentally. The principal g tensor components of Ce^{3+} pair centers are also calculated. Nevertheless, it was impossible to assign each of the satellite lines to actual positions of the six NN and 12 NNN Ce pairs in the lattice due to lack of valid information on the sign of the exchange interactions. The influence of Ce^{3+} pairs on the luminescence efficiency is discussed as well.

DOI: 10.1103/PhysRevB.92.224105 PACS number(s): 61.72.S−, 71.70.Gm, 78.70.Ps, 76.30.Mi

I. INTRODUCTION

Cerium-doped yttrium-aluminum perovskite ($YAlO_3$; YAP has sufficiently high density (about 5.4 g/cm^3), high light yield (about 18 000 photons/MeV), and short decay time (about 30 ns) to make it fit the requirements for γ-ray detection [1]. Trivalent cerium ions, due to the luminescent transition $5d \rightarrow 4f$, act as effective emission centers in these crystals [2,3]. The scintillator is sufficiently fast and mechanically and chemically resistant. Its good mechanical properties allow precise processing. A very weak afterglow makes $YAlO_3$ advantageous in imaging applications. YAP:Ce-based scintillation detectors are widely used for x- and γ-ray counting, electron microscopy, and electron and x-ray imaging screens. Additionally, mixed (Y,Lu)AlO_3:Ce single-crystal scintillators with higher density and effective atomic number have been used as γ-ray detectors in positron emission tomography [4–9].

The scintillator which is of interest in the present work belongs to the class of the so-called activated crystals. Deep understanding of cerium incorporation and its distribution inside the crystal is therefore essential. In this respect, electron paramagnetic resonance (EPR) provides unique microscopic information about characteristics of paramagnetic centers of different origins in a lattice [10].

Previous EPR studies of Ce-doped YAP were devoted to the description of single-ion Ce^{3+} spectra [11,12]. In particular, the g factors of the Ce^{3+} ions and g factors as well as the constants of hyperfine interactions of background Nd^{3+} and Er^{3+} impurities have been obtained from the EPR study of $YAlO_3$:Ce. All rare-earth ions were reported to substitute for the Y host ions. Accuracy of the g tensors and hyperfine interaction constants for Ce^{3+}, Er^{3+}, and Nd^{3+} has been improved in further EPR investigations of the $YAlO_3$:Er,Ce,Nd crystals [12]. The authors also reported observation of a number of weak satellite lines with angular dependencies similar to those of the main strong Ce^{3+} resonances.

We have already studied the incorporation of Ce^{3+} ions in $Lu_3Al_5O_{12}$ (LuAG lutetium aluminum garnet) scintillation crystals [13,14]. In contrast to YAP, only a few Ce^{3+} satellite lines are present in the Ce^{3+} EPR spectra of LuAG, which were attributed to three irregular Ce^{3+} centers. The angular dependencies of the satellite spectra are substantially different from those of the main Ce^{3+} spectrum. One of the irregular Ce centers was interpreted as the Ce^{3+} at the Lu^{3+} site with an adjacent Lu_{Al} antisite defect. The other two centers correspond to Ce^{3+} at an Al site without or with an adjacent defect at the Lu site. It should be noted that shallow electron traps Lu_{Al} associated with Lu_{Al} antisite defect centers have been found responsible for the slow tail of the scintillation response and, consequently, a strong deterioration of scintillation performance [15]. The presence of Y at Al sites (Y_{Al} antisite ions) in YAP was directly proved by NMR [16,17]. However, the situation with Ce irregular centers in YAP is still not completely clear. In contrast to LuAG, Ce^{3+} EPR spectra in YAP are very complex. Besides the main resonance lines attributed to unperturbed Ce^{3+} ions, there is a number (more then 20) of satellite lines around each main line. These satellite lines were previously tentatively ascribed to the Ce^{3+} ions perturbed by defects [11,12]. It was assumed that these defects very likely belong to the Y^{3+} ions substituting for the Al^{3+} ions (Y_{Al} antisite ions) as in LuAG. However, so far their origin has not been convincingly evidenced. It is worth noting that similar satellite lines were observed in the mixed $Y_{0.7}Lu_{0.3}AlO_3$:Ce scintillator [18], where they have been referred to as the doublets of lines produced by the coupled Ce^{3+}-Ce^{3+} ions (pairs). However, no thorough classification of the revealed pairs was given in that work.

The present work is focused on the accurate study and rigorous classification of the Ce^{3+} centers in YAP crystals. In particular, we clarify the origin of the satellite lines in the Ce^{3+} EPR spectra. We show that almost all satellite lines exhibit the behavior of doublets originating from the coupled

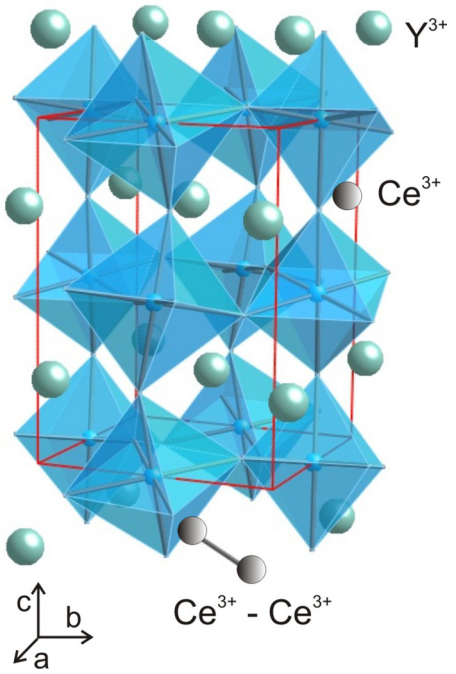

FIG. 1. (Color online) Crystal structure of YAP crystal constructed from AlO_6 octahedrons. Substitution of Ce^{3+} impurity ions for Y^{3+} in the form of the Ce^{3+} single-ion center and the Ce^{3+} - Ce^{3+} nearest-neighbor pair is shown. The crystal axes **a**, **b**, and **c** coincide with the crystallographic directions [100], [010], and [001], respectively.

electron spins of the Ce^{3+}-Ce^{3+} pairs. The experimentally determined spectroscopic parameters are compared with those calculated in the framework of the density functional theory (DFT) adopted by us for calculation of crystal field parameters of rare-earth ions [19].

II. SAMPLES AND EXPERIMENTAL DETAILS

YAP crystallizes in the orthorhombic perovskite structure, space group $D_{2h}^{16}(Pbnm)$ [20] schematically shown in Fig. 1. The lattice parameters are $a = 0.5180$ nm, $b = 0.5330$ nm, and $c = 0.7375$ nm. The four primitive orthorhombic cells contain four pseudoperovskite cells which offer four magnetic sites for substitutional impurity ions for both Al^{3+} and Y^{3+} cations. The Al^{3+} ions occupy positions in the center of a weakly distorted octahedron composed of six oxygen ions. The point group of the aluminum site possesses the inversion symmetry. The Y^{3+} ions are located between oxygen octahedrons (Fig. 1). They possess a mirror symmetry plane (001) and are bound by an inversion through the Al^{3+} sites. Therefore, only two magnetically inequivalent positions for paramagnetic species placed at Y sites can be distinguished when the external magnetic field is rotated in the (001) plane. In the other two orthogonal planes, all four positions are expected to be magnetically equivalent and consequently they cannot be resolved by EPR measurements. The main crystallographic parameters of YAP can be found, e.g., in Ref. [20].

YAP:Ce single crystals were grown by Crytur (Czech Republic) from the melt by the Czochralski method in a Mo crucible in a reducing atmosphere using the charge-containing Y_2O_3, CeO_2 (99.999% purity) and Al_2O_3 (99.99%) oxides. The content of Ce in YAP was 0.5 at. %. In addition, some of the YAP:Ce single crystals were grown with much lower (about 100 times) concentration of the Ce^{3+} ions.

EPR spectra were acquired with a Bruker *X*-/*Q*-band E580 FT/CW ELEXSYS spectrometer at the *X* and *Q* bands with the microwave frequencies 9.4 and 34 GHz at a temperature of 18–20 K. The crystals were cut in three orthogonal planes (*ab*),(*ac*), and (*bc*) with the size $6 \times 2.2 \times 2.2\,\text{mm}^3$ for measurements at the *X* band and in the (*ab*) and (*ac*) planes with the size $2 \times 1.2 \times 1.2\,\text{mm}^3$ for *Q*-band measurements. The angular dependencies of the Ce^{3+} spectra were measured by rotating the sample mounted on a quartz holder around reference axes in steps of 2°. The accuracy of the crystal orientations on the quartz holder was about 1° and 2°. At the *X* and *Q* bands, respectively.

III. EXPERIMENTAL RESULTS

A. Single-ion Ce^{3+} center

The Ce^{3+} ion has an outer electronic shell configuration $4f^1$ ($S = 1/2$). Taking into account that the ionic radius of Ce^{3+} (1.01 Å) in the sixfold oxygen coordination is almost twice larger compared to the ionic radius of Al^{3+} (0.535 Å) [21], the Ce^{3+} is expected to substitute for Y^{3+} (Fig. 1), whose ionic radius in the 12-fold oxygen coordination is approximately 1.24 Å compared with 1.34 Å for that of Ce^{3+} for the same coordination number.

The EPR spectrum measured in YAP:Ce with the external magnetic field running along the crystallographic direction **a** is shown in Fig. 2. It contains contributions from a strong single line labeled as 1 and a number of weak satellite lines (lines 2–8) almost symmetrically located around the main resonance line with a total intensity of about 10% of the intensity of the central line. The strong line is produced by single Ce^{3+} ions [the Ce(I) center] in accordance with published data [11,12].

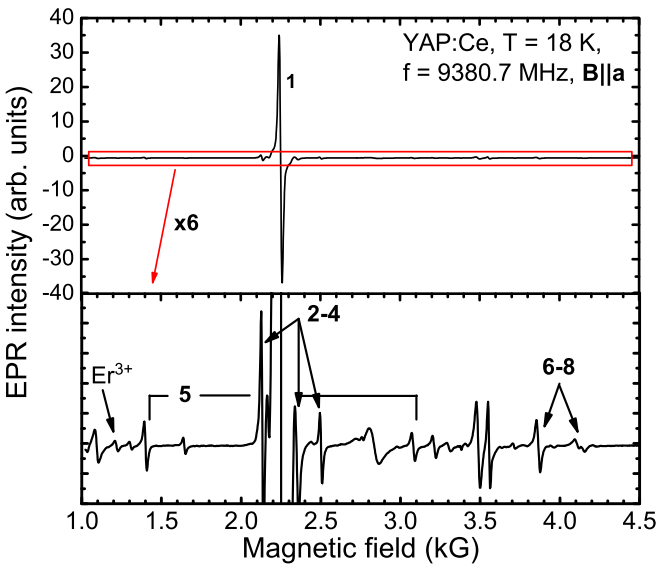

FIG. 2. (Color online) EPR spectrum of Ce^{3+} ions measured in YAP:Ce single crystal with the orientation of the external magnetic field **B**||**a** at the temperature 18 K. 1 denotes the single-ion Ce(I) spectral line, 2–8 are spectral lines from the Ce^{3+}-Ce^{3+} pairs. The intensity of the spectrum in the bottom panel is multiplied by 6.

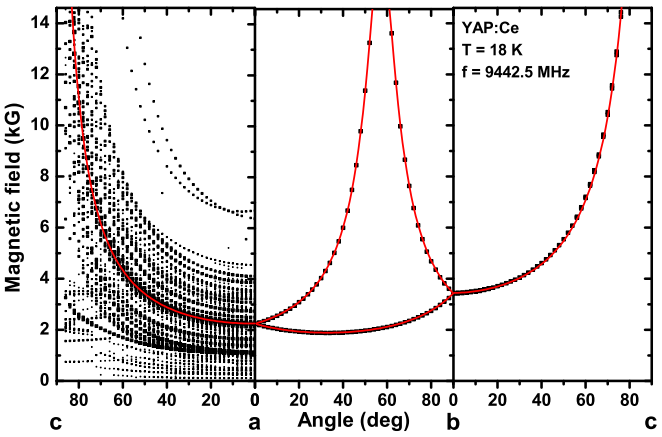

FIG. 3. (Color online) Angular dependencies of the Ce(I) magnetic resonance fields measured in the (ac),(ab), and (bc) planes. Solid lines are calculated angular dependencies. Resonance fields of satellite transitions are shown by rectangular dots only for the (ac) plane.

This is a single-ion paramagnetic center, i.e., the Ce^{3+} ions do not influence each other due to the relatively large distance between them. As we will show below, the satellite lines belong to coupled Ce^{3+}-Ce^{3+} ions.

In order to determine the g tensor components and orientations of the magnetic axes of the Ce(I) center, the angular dependencies of the resonance magnetic fields were measured in three orthogonal planes coinciding with the crystallographic planes (ac),(ab), and (bc) (Fig. 3). These angular dependencies were described by the following g factors: $g_x = 0.210$, $g_y = 0.395$, and $g_z = 3.565$, where the **x** axis of the magnetic coordinate system coincides with the **c** crystal axis and the other two axes are located in the (ab) plane. The complete set of spectral parameters of the Ce(I) center is listed in Table I, where previously reported g tensor components are presented as well. One can see that two of the g factors, $g_y = 0.395$ and $g_z = 3.565$, are close to those reported in [11,12]. However, the $g_x = 0.21$ is almost twice smaller than that reported previously. Our careful measurements at high magnetic fields, up to 14.6 kG, show that such a steep change of the resonance field in the direction close to the **c** crystal axis cannot be described by $g \approx 0.4$. It needs a much smaller g factor. It should be noted that the resonance lines are also slightly split into two components in the (ac) and (bc) planes. The spectral spacing between the two lines increases by up to 200–300 G at angles close to the **c** direction (Fig. 3). This means that the **x** magnetic axis is not exactly parallel to the **c** crystal axis (the deviation is 1°), probably due to a small mismatch in crystal orientation. In the fitting procedure we ignored this fact and the theoretical curves shown in Fig. 3 were calculated assuming a coincidence of the **x** magnetic axis with the **c** crystal direction. A good coincidence of the experimental data with those calculated in three rotational planes confirms that the determined spin Hamiltonian parameters correctly describe the Ce(I) center.

B. Ce^{3+}-Ce^{3+} pair centers

1. EPR spectra

In the Ce^{3+} spectrum shown in Fig. 2, in addition to the resonance line corresponding to the main Ce(I) center, many satellite lines are present as well. In previous work [12] dealing with the study of the Ce^{3+} ions in YAP:Ce these satellite lines were intuitively ascribed to Ce^{3+} ions with a somewhat distorted environment. However, the satellite lines are almost symmetrically placed with respect to the central strong line of the Ce(I) center throughout the angular variations (Fig. 3). This peculiarity could hardly be explained only by distorted surroundings of cerium ions, which induces changes in the g tensor. It rather suggests the presence of doublets originating from coupled Ce^{3+}-Ce^{3+} ions. To check this possibility, we performed measurements of the spectra at the Q microwave band (34 GHz). Surprisingly, we obtained a similar spectrum with approximately the same distances between satellite lines but with much better resolution than that at the X band, especially at low magnetic fields (Fig. 4), due to the approximately four times larger Zeeman energy at the Q band. Moreover, the corresponding angular dependencies of the doublet resonance positions (Fig. 5) repeat the angular dependencies of the main Ce(I) center. This indicates that the satellite spectra indeed belong to Ce^{3+}-Ce^{3+} coupled ions and have to be described by a spin Hamiltonian that includes the spin-spin interaction.

Two identical Ce^{3+} ions coupled by the spin-spin interaction will give rise to four states in the spin system having values of the total effective spin $S = S_1 + S_2$ of 0 and 1. EPR transitions could be observed only within the $S = 1$ triplet states [22]. Two identical Ce^{3+} ions will therefore give rise to a spectrum of only two lines for a given magnetic field direction. The transitions can be described by the spin Hamiltonian [22]

$$\mathbf{H} = \beta_e \mathbf{S}_1 \mathbf{g}_1 \mathbf{B} + \beta_e \mathbf{S}_2 \mathbf{g}_2 \mathbf{B} + K_x S_{1x} S_{2x} + K_y S_{1y} S_{2y} + K_z S_{1z} S_{2z}, \quad (1)$$

where $\mathbf{S}_1$, $\mathbf{S}_2$, $\mathbf{g}_1$, and $\mathbf{g}_2$ are the spin operators and g tensors of both Ce^{3+} ions of a pair, β_e is the Bohr magneton, and K_i are the spin-spin interaction constants including the contribution from both the dipole-dipole and exchange interactions. The spin Hamiltonian (1) assumes that both g and spin-spin interaction tensors have the same principal axes, which is obviously valid only for magnetically equivalent (ME) nearest neighbor (NN) pairs. Only two of six such pairs exist in the NN location (Fig. 6). The other four NN pairs interact as magnetically nonequivalent (MNE) ions. For them, along with the next-nearest-neighbor (NNN) pairs, small off-diagonal terms in the spin Hamiltonian are expected as well.

It is appropriate to analyze the angular dependence of the doublets in the (ac) rotational plane by plotting the resonance fields multiplied by $\cos\theta$, where θ is the angle between the external magnetic field and the **a** axis. Such data are shown in Fig. 7. This graph clearly demonstrates that the doublets almost perfectly repeat the angular variation of the main resonance line, including even a small splitting of this line at angles near the **a** axis, except for two pairs of lines which show splitting when the magnetic field deviates from the **a** crystal direction. This observation implies that the g tensors of pair centers do not significantly differ from that of the single ion and off-diagonal terms are negligibly small.

The data presented in Fig. 7 can be understood in the following way. Because one of the g tensor components, namely, g_z, is much larger than the other two components ($g_x/g_z \sim 0.05$; $g_y/g_z \sim 0.1$), we can assume that there is an

TABLE I. Spectral characteristics and relative concentrations of the Ce^{3+} centers in YAP:Ce crystals obtained from the EPR data. The principal axis orientations of g and spin-spin interaction tensors are given by the Euler angle α which defines the deviation of the principal axis **z** from the crystal axis **a** in the (ab) plane. The error margin of the Euler angle is approximately 2°.

Center	g factors	K tensor components (cm^{-1})	Euler angle (deg)	Relative concentration
Ce(I)	$g_x = 0.210 \pm 0.005$			
	$g_y = 0.395 \pm 0.005$		$\alpha = \pm 32.8$	90%
	$g_z = 3.565 \pm 0.005$			
Ce(I) Ref. [12]	$g_x = 0.395$			
	$g_y = 0.402$		$\alpha = \pm 31.8$	
	$g_z = 3.614$			
Ce2	$g_x = 0.181 \pm 0.005$	$\lvert K_x \rvert = 0.005 \pm 0.005$		
	$g_y = 0.391 \pm 0.005$	$\lvert K_y \rvert = 0.010 \pm 0.005$	$\alpha = \pm 33$	0.85%
	$g_z = 3.590 \pm 0.005$	$\lvert K_z \rvert = 0.047 \pm 0.005$		
Ce3	$g_x = 0.181 \pm 0.005$	$\lvert K_x \rvert = 0.007 \pm 0.005$		
	$g_y = 0.391 \pm 0.005$	$\lvert K_y \rvert = 0.020 \pm 0.005$	$\alpha = \pm 33.5$	2.6%
	$g_z = 3.590 \pm 0.005$	$\lvert K_z \rvert = 0.095 \pm 0.005$		
Ce4	$g_x = 0.20 \pm 0.01$	$\lvert K_x \rvert = 0.01 \pm 0.01$		
	$g_y = 0.391 \pm 0.005$	$\lvert K_y \rvert = 0.03 \pm 0.01$		
	$g_z = 3.632 \pm 0.005$	$\lvert K_z \rvert = 0.10 \pm 0.01$		1.6%
Ce5	$g_x = 0.158 \pm 0.005$			
	$g_y = 0.412 \pm 0.005$		$\alpha = \pm 33$	0.3%
	$g_z = 3.599 \pm 0.005$	$\lvert K_z - (K_x + K_y)/2 \rvert = 0.165$		
Ce6	$g_x = 0.181 \pm 0.005$			
	$g_y = 0.391 \pm 0.005$		$a = \pm 33$	1%
	$g_z = 3.592 \pm 0.005$	$\lvert K_z - (K_x + K_y)/2 \rvert = 0.22$		
Ce7	$g_x = 0.158 \pm 0.005$			
	$g_y = 0.412 \pm 0.005$		$\alpha = \pm 33.5$	0.5%
	$g_z = 3.580 \pm 0.005$	$\lvert K_z - (K_x + K_y)/2 \rvert = 0.29$		
Ce8	$g_x = 0.158 \pm 0.005$			
	$g_y = 0.412 \pm 0.005$			
	$g_z = 3.620 \pm 0.005$	$\lvert K_z - (K_x + K_y)/2 \rvert = 0.43$		0.6%
Ce9	$g_x = 0.211 \pm 0.005$	$\lvert K_x \rvert = 0.036 \pm 0.005$		
	$g_y = 0.401 \pm 0.005$	$\lvert K_y \rvert = 0.038 \pm 0.005$	$\alpha = \pm 33$	1.1%
	$g_z = 3.620 \pm 0.005$	$\lvert K_z \rvert = 0.54 \pm 0.01$		
Ce10	$g_x = 0.211 \pm 0.005$	$\lvert K_x \rvert = 0.033 \pm 0.005$		
	$g_y = 0.401 \pm 0.005$	$\lvert K_y \rvert = 0.05 \pm 0.005$	$a = \pm 33$	0.8%
	$g_z = 3.565 \pm 0.005$	$\lvert K_z \rvert = 0.57 \pm 0.01$		
Ce11	$g_x = 0.211 \pm 0.005$	$\lvert K_x \rvert = 0.03 \pm 0.005$		
	$g_y = 0.401 \pm 0.005$	$\lvert K_y \rvert = 0.07 \pm 0.005$	$\alpha = \pm 33$	0.4%
	$g_z = 3.578 \pm 0.005$	$\lvert K_z \rvert = 0.65 \pm 0.01$		

axial symmetry of the g tensor and spin-spin interaction. Consequently, we can obtain an approximate expression for EPR transitions of pairs in the (ac) plane by applying a perturbation theory to the spin Hamiltonian (1). Up to the second order they are given by the expression

$$h\nu = g_z \beta_e B^{\pm} \cos\theta \, \cos\alpha \pm \frac{1}{2}(K_z - K_\perp) + \frac{1}{2h\nu} g_\perp^2 \beta_e^2 (B^{\pm})^2 (\sin\theta + \cos\theta \, \sin\alpha)^2, \quad (2)$$

where $B^{\pm}$ denote the two resonance fields of the pair spectra, $K_\perp$ and $g_\perp$ denote the mean values of K_x, K_y and g_x, g_y, respectively, and α is the angle between the principal **z** axis and the **a** axis. These resonances are approximately symmetrically placed around the main resonance line and separated by $(K_z - K_\perp)/2 g_z \beta_e \cos\theta \, \cos\alpha$ from it. Therefore they should show an angular variation similar to that of the single-ion spectral line, and the difference $K_{zz} - K_\perp$ can be easily determined from the doublet positions.

Precise values of the spin-spin interaction tensor components were determined from a simulation of the angular dependencies of the resonance fields of the Ce^{3+} pair centers using numerical diagonalization of the spin Hamiltonian (1). The simulated angular dependencies are shown in Figs. 5 and 7 by solid lines. The determined spin-spin coupling constants and g tensor components of the identified Ce^{3+} pair centers are listed in Table I. Note that only the differences $|K_z - (K_x + K_y)/2|$ could be determined for the Ce5-Ce8 pairs. For most of the pair centers $K_z \gg K_x, K_y$ and the doublet positions mainly depend on the K_z component of the K_{ij} tensor. This is because the anisotropy of the spin-spin interaction, both dipole-dipole and exchange, is proportional to the g factor anisotropy approximately as $(g_z/g_x, g_y)^2$ [23]. The selection of the signs of the spin-spin interaction constants will be discussed shortly.

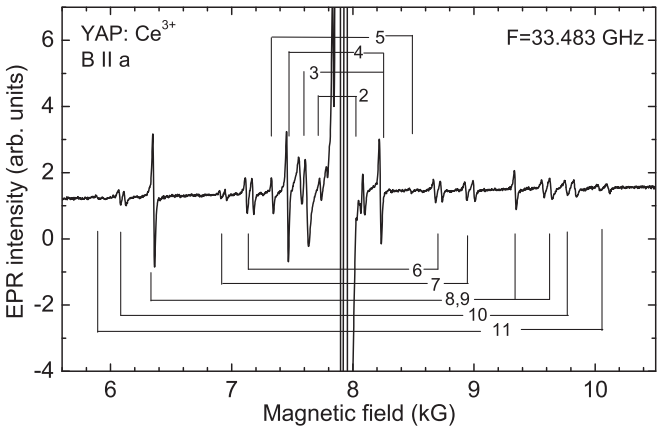

FIG. 4. EPR spectrum of Ce^{3+} ions measured in YAP:Ce single crystal with the orientation of the external magnetic field **B**||**a** at the frequency 33.48 GHz and temperature 22 K. The strong line corresponds to the main Ce(I) center; doublets 2–11 correspond to Ce^{3+} pair centers.

2. *Spectral intensity analysis*

The intensities of the spectral lines of the Ce^{3+} pairs are proportional to the probability of finding two Ce^{3+} ions at a given distance. We can consider a simple model with the reference Ce^{3+} ion in the center of a lattice constructed only of Y ions [Fig. 6(a)]. There are six NN Y sites in the first coordination sphere associated with the reference Ce site. The second and third coordination spheres contain 12 and 8 NNN Y sites separated by the edge and face diagonals, respectively. Taking into account a small concentration of Ce ions and assuming their random distribution in the lattice,

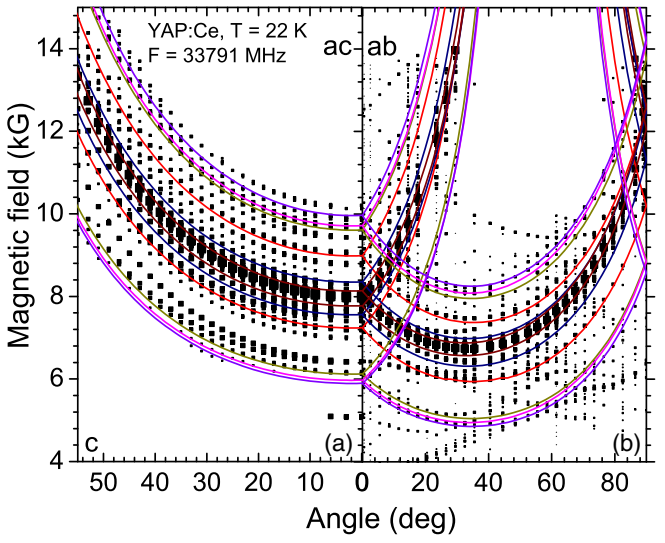

FIG. 5. (Color online) Angular dependencies of Ce^{3+} resonance fields measured in the (*ac*) and (*ab*) planes at the frequency 33.79 GHz and temperature 22 K. Solid lines are calculated angular dependencies of pair centers. Rectangular dots represent experimental data (the size of the dots is proportional to the logarithm of the intensity of EPR lines in the spectra).

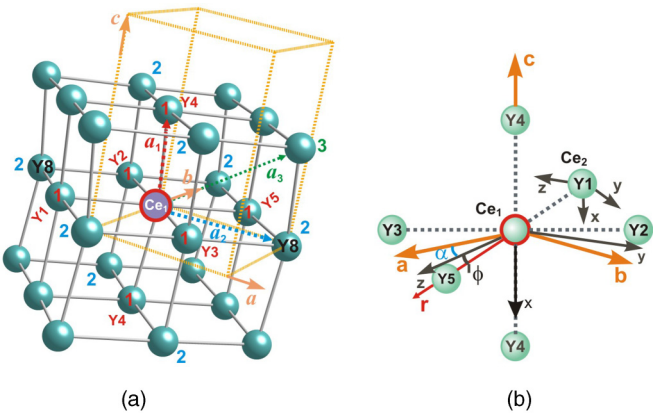

FIG. 6. (Color online) (a) Y^{3+} sublattice with the Ce_1 ion in the center (only Y lattice sites are shown). The second Ce_2 ion of a pair is located at any of the six NN Y sites (distance $a_1 \approx 3.8$ Å; ions are labeled from Y1 to Y5) or NNN Y sites separated by the edge (distances $a_2 \approx 5.6$ Å; two equivalent Y8 sites are indicated) or space diagonals (distances $a_3 \approx 6.5$ Å), respectively. (b) Ce-Ce NN pairs are shown separately. Y1–Y3, Y5, and Y4 designate MNE and ME ions, respectively. **x**,**y**,**z** are g tensor principal axes of the reference ion Ce_1 and MNE second ion Ce_2. $\alpha = 32.8^\circ$ and $\phi = 12^\circ$ are the Euler angle and the deviation of the line **r** connecting two ions from the principal **z** axis in the (ab) plane.

the probability $P_i(m)$ for a given Ce-occupied Y site to be accompanied by m Ce ions anywhere in the ith coordination

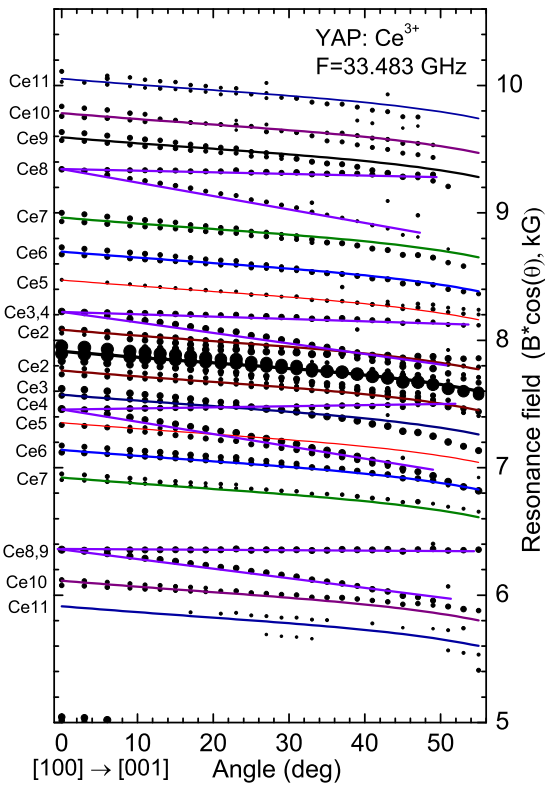

FIG. 7. (Color online) Angular variation of the Ce^{3+} resonance fields multiplied by cosθ in the (ac) plane and frequency 33.48 GHz. The solid lines are calculated using parameters listed in Table I for different Ce^{3+} pairs designated from Ce2 to Ce11.

TABLE II. Probabilities $P_i(m)$ for a given Ce-occupied Y site to be accompanied by m Ce ions anywhere in the ith coordination sphere.

Coordination sphere number i	1	2	3
Number of Y sites n_i	6	12	8
$P_i(x=0)$	97.04%	94.16%	96.07%
$P_i(x=1)$	2.93%	5.68%	3.86%

sphere is given by the binomial distribution function

$$P_i(m) = \binom{n_i}{m} p^m (1-p)^{n_i - m}, \tag{3}$$

where $p = 0.005$ is the total concentration of Ce^{3+} ions in the material and n_i is the number of positions in each coordination sphere.

The probabilities $P_i(m=0)$ and $P_i(m=1)$ calculated for each n_i are listed in Table II. Figure 6(a) shows three coordination spheres around the reference Ce ion. The next, fourth, coordination sphere, is composed of 38 ions situated at double the Y-Y interatomic distances. Obviously, all Ce ions separated by distances larger than twice the Y-Y distance can be considered as single paramagnetic ions since the spin-spin interaction between them is smaller than or comparable to the intrinsic linewidth. It will be shown below that only pairs from the first two coordination spheres produce distinguishable contributions to the spectrum. The total concentration of these pairs is 2.93%(NN) + 5.68%(NNN) = 8.61%. The probability of finding no other cerium ion simultaneously in the first two levels is equal to 91.39%. These two values predict the relative concentrations of the pair centers and the single-ion Ce(I) center, respectively.

The relative concentrations of the Ce^{3+} centers have been estimated from the integral intensities of the corresponding EPR lines at the crystal orientation **a** parallel to the external magnetic field (Fig. 4), where the resonance lines of two magnetically inequivalent centers almost coincide. The population of the single Ce(I) center is found to be about 90%, slightly smaller than the calculated value. The relative concentration of all visible pair centers is consequently about 10%. Individual concentrations of all identified centers are listed in Table I.

Finally, to unambiguously confirm that the studied Ce^{3+} centers genuinely correspond to ionic pairs, EPR spectra in samples with the concentration of Ce^{3+} ions about 100 times smaller were measured. At such a low concentration of paramagnetic ions (0.005 at. %), the probability of finding an ionic pair at a short distance is negligibly small and the spectra of pair centers should not be observed. Corresponding spectra acquired at two orientations of the external magnetic field are shown in Fig. 8. One can see that no satellite lines are visible around the main Ce^{3+} lines.

The spectral intensity analysis does not allow distinguishing pair centers belonging to a pair of nearest-neighbor or next-nearest-neighbor Ce^{3+} ions alone, as the populations of different pair centers are not too different. It rather provides an overall qualitative agreement of the considered model with experimental data. The assignment of the observed spectra to different pair centers can, in principle, be done by analyzing the spin-spin coupling constants.

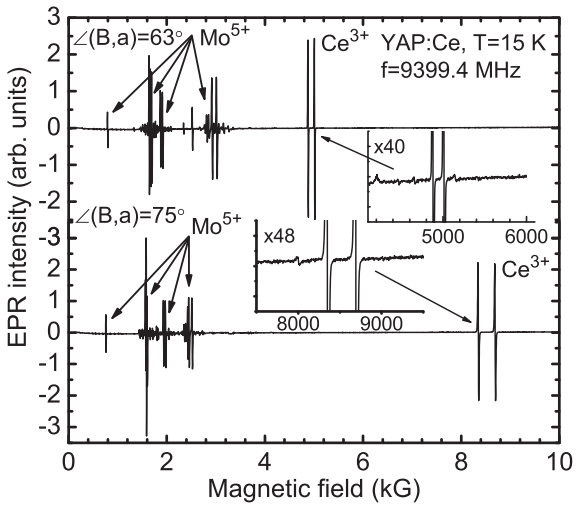

FIG. 8. EPR spectra of Ce^{3+} ions measured in weakly (0.005 at. %) doped YAP:Ce single crystal. The spectral lines from Mo^{5+} are identified as well.

3. Spin-spin interaction

The spin-spin coupling constant K originates from the dipole-dipole and exchange interactions. Of these two interactions, the energy of the dipole interaction is the one most predictable. Moreover, in the case of rare-earth ions, it can be comparable to or even larger than that of the exchange energy [22,23]. The constant (energy) of the dipole-dipole interaction for magnetically equivalent ions is given by the following expression [22]:

$$K_d = \beta_e^2 r^{-3} \begin{bmatrix} \langle 1-3l^2\rangle g_x^2 & -\langle 3lm\rangle g_x g_y & -\langle 3nl\rangle g_x g_z \\ -\langle 3lm\rangle g_x g_y & \langle 1-3m^2\rangle g_y^2 & -\langle 3mn\rangle g_y g_z \\ -\langle 3nl\rangle g_x g_z & -\langle 3mn\rangle g_y g_z & \langle 1-3n^2\rangle g_z^2 \end{bmatrix}, \tag{4}$$

where K_d is the dipolar interaction tensor, r is the distance between ions in the pair; g_i are corresponding components of the g tensor ($i = x,y,z$), and l,m,n are the direction cosines of the vector **r** which connects two Ce ions.

Because of the large anisotropy of the g values ($g_x/g_z \sim 0.05$; $g_y/g_z \sim 0.1$), there is a significant contribution only to the K_z component. Its value can be easily determined from the known distances r between Ce ions in the pair and the direction cosines of the vector **r**. Let the reference ion be placed at the origin of the Cartesian axis system (see Fig. 6). There are six nearest positions for the second Ce ion, with the distances between ions $r_1 = 3.64$ Å, $r_2 = 3.79$ Å (altogether four MNE ions, Y1–Y3 and Y5 in Fig. 6), and $r_3 = 3.73$ Å (two ME ions, Y4, in Fig. 6) within the first coordination sphere of radius $a_1 = 3.8$ Å. To calculate the dipolar interaction constant of the ME ions the values of corresponding g tensor components from Table I were introduced into Eq. (4). This gives $K_{dz} = g_z^2 \beta_e^2 r_3^{-3} = 0.106\,\mathrm{cm}^{-1}$ for both pairs of ME ions.

Equation (4) is slightly changed in order to describe the dipolar interaction between magnetically nonequivalent NN ions as the two principal axes of their g tensor do not coincide.

It has the following form:

$$K_{dd} = \beta_e^2 r^{-3} \begin{bmatrix} \langle 1-3l^2\rangle g_x g_y & -\langle 3lm\rangle g_x^2 & -\langle 3nl\rangle g_x g_z \\ -\langle 3lm\rangle g_y^2 & \langle 1-3m^2\rangle g_x g_y & -\langle 3mn\rangle g_y g_z \\ -\langle 3nl\rangle g_y g_z & -\langle 3mn\rangle g_x g_z & \langle 1-3n^2\rangle g_z^2 \end{bmatrix}, \quad (5)$$

Four positions of MNE ions with respect to the reference Ce_1 ion give two sets of dipolar tensor components according to the orientation of the line connecting two MNE ions. The tensor (5) is, in general, not diagonal. Nevertheless, the off-diagonal terms together with K_{dx} and K_{dy} do not exceed 7% and 14% of the largest K_{dz} value given by $g_z = 3.565$. They were neglected in our analysis as they could hardly be determined from the spectra. Then $K_{dz} = \langle 1 - 3\cos^2(\xi + \phi)\rangle g_z^2 \beta_e^2 r_{1,2}^{-3}$, where $\xi = n\pi/2$ ($n = 0,1,2,3$ for each of the MNE ions), and $\phi = 12^\circ$ is the deviation of the line connecting two ions from the principal **z** axis of the reference ME ion. Taking into account the mutual orientation of the ions in each MNE pair, for the $r_{1,2}$ distances the respective values of the dipolar interaction tensor z components are $K_{dz}^1 = 0.099$ and $-0.213\,\mathrm{cm}^{-1}$ [pairs Y2 and Y5 in Fig. 6(b)] and $K_{dz}^2 = -0.189$ and $0.088\,\mathrm{cm}^{-1}$ (pairs Y1 and Y3).

The Ce-Ce distances for the second Ce ion at the second coordination sphere (next-nearest neighbors) are 5.33, 5.18, 4.97, and 5.54 Å within the radius $a_2 = 5.6$ Å. They determine six different types of pairs with ions located at the face diagonals [Fig. 6(a)]. Since the dipolar interaction ($\sim r^{-3}$) is expected to be much weaker in that case, the corresponding dipolar constants were estimated only using Eq. (4). They are $K_{dz}^1 = -0.0182\,\mathrm{cm}^{-1}$, $K_{dz}^2 = -0.0198\,\mathrm{cm}^{-1}$, $K_{dz}^3 = -0.0224$ and $0.0448\,\mathrm{cm}^{-1}$, $K_{dz}^4 = -0.0162$ and $0.0324\,\mathrm{cm}^{-1}$. For the third coordination sphere, the Ce-Ce distances are 6.531 and 6.363 Å within the radius $a_3 = 6.5$ Å. The dipolar constants are smaller than $10^{-4}\,\mathrm{cm}^{-1}$. At such distances, the exchange interaction is negligibly small as well. The resonance lines originating from these types of pairs are totally superimposed on a single strong line in the spectrum. Therefore, such pairs will be excluded from further consideration. On the other hand, they contribute to the intensity of the central line, causing some difference between calculated and experimentally determined concentrations of Ce^{3+} centers. It should be noted that we used unrelaxed positions of Ce^{3+} ions in the calculation of the dipole interaction energies. Our DFT calculations (Sec. 4, Table III, below) show that the distances between Ce^{3+} ions do not substantially change when relaxation of lattice produced by the incorporation of Ce ions at Y sites is allowed.

The spin-spin coupling constant K is the sum of the dipolar constant, given by Eqs. (4) and (5), and the exchange energy J. These two contributions are usually comparable in absolute value for Ce^{3+} ions [22,23]. For instance, J is about $0.2\,\mathrm{cm}^{-1}$ for both nearest and next-nearest neighbors in $LaCl_3$ [24]. Therefore, it is problematic to derive exchange constants from EPR data. We can argue that their magnitude can be larger than that in $LaCl_3$ due to the shorter distance between Ce ions. Unfortunately, the sign of the spin-spin interaction could not be determined experimentally from the relative intensities of the transitions at low temperatures as the spectra are completely saturated already at the temperature 6–8 K due to the long spin-lattice relaxation time. We can only assume that the exchange interaction between Ce ions is of antiferromagnetic type for NNs and ferromagnetic for NNNs, similar to that in $LaCl_3$ and between Eu^{2+} ions in the cubic perovskite $EuTiO_3$ [25]. However, in general, the problem of the exchange interaction of Ce^{3+} ions is quite complex due to the essential anisotropy in the spin-spin interaction and is not resolved yet as no magnetic materials based on Ce^{3+} ions exist. The present precision of DFT calculations does not allow determination of the exchange energies of single Ce^{3+} pairs either.

TABLE III. Positions (NN and NNN) for the second Ce^{3+} ion site (Ce_2) with fixed first Ce^{3+} ion (Ce_1) of the Ce-Ce pair. Positions in Å are obtained as (*Aa*, *Bb*, *Cc*), where *a*,*b*,*c* are the lattice parameters of YAP.

Substitutional Y (Ce_2) site	***A***	***B***	***C***	**Ce_1 − Y(Ce_2) distance (Å)**
Y 1	−0.242	0.755	0.000	3.62
Y 2	−0.239	1.258	0.000	3.72
Y 3	0.263	0.759	0.000	3.72
Y 4	0.010	0.954	−0.252	3.74
Y 4	0.010	0.954	0.252	3.74
Y 5	0.262	1.260	0.000	3.88
Y 6	0.249	1.205	−0.251	5.00
Y 6	0.249	1.205	0.251	5.00
Y 7	−0.252	1.204	−0.250	5.03
Y 7	−0.252	1.204	0.250	5.03
Y 8	0.496	1.009	0.000	5.12
Y 9	−0.002	0.508	0.000	5.23
Y 8	−0.504	1.009	0.000	5.24
Y 9	−0.002	1.508	0.000	5.43
Y 10	0.247	0.705	−0.250	5.47
Y 10	0.247	0.705	0.250	5.47
Y 11	−0.251	0.705	0.250	5.50
Y 11	−0.251	0.705	−0.250	5.50

The ferromagnetic interaction between NNNs can be even stronger compared to that between NNs. For instance, the ratio J_{NNN}/J_{NN} is about 2 in $EuTiO_3$. Therefore, it is reasonable to ascribe some of the pairs with the largest K_z values, the Ce8–Ce11 pairs in Table I, to next-nearest neighbors. For these pairs, the dipole contribution to the coupling constant K is negligibly small. The J_{NNN} energies are thus $\approx$0.40–0.6 cm^{-1} depending on the Ce-Ce distance, which varies from 4.97 to 5.54 Å. The Ce8 center shows splitting of spectral lines when the magnetic field rotates in the (ac) plane (Fig. 7). This splitting is caused by a small deviation of the **x** principal axis of the g tensor from the **c** crystal direction due to the appearance of g_{zx} components, indicating local distortion along the [101] direction that coincides with the Ce-Ce connecting line. However, the precise orientation of the principal axes of this center and the similar center Ce4 could not be determined as their resonances in the (ab) plane are completely masked by resonances from other centers. For these two centers we ignored the splitting in the spectrum in the calculation of the coupling constant K_z which obviously does not significantly increase the error.

Assuming that the NN interaction between Ce ions is comparable to or even weaker than the NNN interaction, its value can reasonably be in the range $|J_z| \sim (0.2 - 0.3)\ \mathrm{cm}^{-1}$

depending on the Ce-Ce distance. The combination of the exchange interaction with the dipole-dipole interaction, which changes from 0.1 to $-0.23\,\mathrm{cm}^{-1}$, gives a broad range of possible values (from -0.4 to $0.1\,\mathrm{cm}^{-1}$) of the spin-spin coupling constant for nearest neighbors. Obviously, most of the centers with small coupling constants belong to NNs. However, a practically uniform distribution of the satellite lines in the magnetic field range of 6–10 kG makes it impossible to assign each of the satellite lines to actual positions of the 6 NN and 12 NNN Ce-Ce pairs in the lattice.

C. Calculation of the *g* tensor with Wannier functions

During the last three years we developed a different method to calculate the crystal field parameters of the rare-earth ions in solids. The method starts with a density-functional-theory-based band structure calculation, followed by a transformation of the Bloch to the Wannier basis. The local Hamiltonian is then expanded in terms of the spherical tensor operators. The resulting crystal field parameters are inserted in an atomiclike Hamiltonian involving the crystal field, $4f$ electron correlation, spin-orbit coupling, and Zeeman interaction. The hybridization of the $4f$ states with ligand orbitals is taken into account via a hybridization parameter Δ, which is estimated independently [26].

So far the method has been applied to more than 60 rare-earth- (*R*-) containing compounds: multiplet splitting of *R* impurities in $YAlO_3$ [19] and LaF_3 [26], in the yttrium as well as the lutetium aluminum garnets [27]; and in the orthorhombic perovskites $RGaO_3$, $RCoO_3$ [28], and $RMnO_3$ [29] the *g* tensor was also determined. The calculated results agree remarkably well with the experiment, the crystal-field-split multiplet levels within a few meV, and the magnetic properties are correctly described as well. In the above listed calculations for perovskites the value of $\Delta = -8.2\,\mathrm{eV}\,(-0.6\,\mathrm{Ry})$ was adopted. The results presented below were obtained with a supercell containing 24 $YAlO_3$ formula units, in which one (two) Y atoms were replaced by Ce in a single-impurity (Ce-Ce pair) calculation. To determine the band structure we first relax the positions of ions in the supercell, while the unit cell parameters are taken from experimental data. We use the WIEN2K package [30] which implements the augmented plane waves + local orbital method. Within this method, the atomic radii for Ce, Y, Al, and oxygen were taken as 2.3, 2.15, 2.15, and 1.64 a.u., respectively. Note that these *atomic* radii are parameters of the computational code and they differ from the *ionic* radii referred to above. The number of basis functions is ~9200, corresponding to the parameter $RK_{\max} = 6.5$; the number of the *k* points in the Brillouin zone was 18.

1. *Single-ion* Ce^{3+} *center*

The crystal field Hamiltonian $\hat{H}_{\mathrm{CF}}$ in the Wybourne notation [31] has the form

$$\hat{H}_{\mathrm{CF}} = \sum_{k=2,4,6} \sum_{q=-k}^{k} B_q^k \hat{C}_q^k, \tag{6}$$

where $\hat{C}_q^k$ is a spherical tensor operator of rank k acting on the $4f$ electrons of the Ce^{3+} ion. The coefficients B_q^k are the crystal field parameters (CFPs). For the hybridization parameter $\Delta = -8.2\,\mathrm{eV}$ the calculated CFPs in cm^{-1} are the following: $B_0^2 = -44.4$; $B_2^2 = 72.3 + 679i$; $B_0^4 = -382$; $B_2^4 = -191 + 857i$; $B_4^4 = 139\text{-}801i$; $B_0^6 = -1164$; $B_2^6 = 122 + 612i$; $B_4^6 = -2208\text{-}90i$; $B_6^6 = 139 + 60i$ (these values are related to the coordinate system specified in [19,28]). Using these CFP values we followed the procedure described in our previous work (see, e.g., [19,26]) and calculated the crystal field sublevels of the $^2F_{5/2}$ and $^2F_{7/2}$ multiplets of the Ce^{3+} ion. They are 0, 349, 571 and 2192, 2655, 2888, $3285\,\mathrm{cm}^{-1}$ for the $^2F_{5/2}$ and $^2F_{7/2}$ multiplets, respectively. The corresponding principal components of the *g* tensor are

$$g_x = 0.0893; \quad g_y = 0.1400; \quad g_z = 3.6880, \tag{7}$$

and the Euler angle $\alpha = -30.1^\circ$. (Note that there are two possible crystallographically equivalent sites for the Ce impurity; for the other site $\alpha = +30.1^\circ$). The dependence of these parameters on Δ is weak. Taking into account that no parameter was used to fit the EPR data, the agreement with the experiment reported above ($g_x = 0.210 \pm 0.005$, $g_y = 0.395 \pm 0.005$, $g_z = 3.565 \pm 0.005$, $|\alpha| = 32.8^\circ$) is satisfactory. In particular, the value g_y is substantially larger than that of g_x and both are much smaller than the g_z value, confirming the outcome of current experimental observations presented in the previous section. Since the angular dependencies of Ce^{3+} resonance fields are mainly affected by the smallest *g* components, the larger error of the g_x and g_y values determined from the experiment is expected. The calculated angle α is also close to its experimental value.

Note that the calculated multiplet splitting of the $^2F_{7/2}$ multiplet is in excellent agreement with that determined experimentally [32]. The location of the energy levels of the $^2F_{5/2}$ multiplet was not determined experimentally. These energies were evaluated by an empirical crystal field analysis based on perturbation theory [33]. This analysis predicts the energy levels at 0, 412.89 and $996.03\,\mathrm{cm}^{-1}$, markedly different from those above obtained from DFT calculation. However, as pointed out above a satisfactory agreement between our calculations and experiment was found for the *g* factors. Since the *g* factors are very sensitive to crystal field splitting, namely, that of the $^2F_{5/2}$ multiplet, our DFT results seem reliable.

2. Ce^{3+} -Ce^{3+} *pair centers*

With the first Ce^{3+} ion (Ce_1) fixed in the (*ab*) plane at $0.001\,42a$,$0.998\,67b$, and $0.000\,00c$, where a,b,c denote the lattice parameters of YAP, possible positions for the second Ce^{3+} ion site (Ce_2) situated closer than 0.7 nm [corresponding to NN and NNN distances; cf. Fig. 6(a)] are listed in Table III. There are thus five inequivalent possible sites for the second Ce^{3+} with distance $r < 0.4$ nm (corresponding to NN sites of the first coordination sphere) and eight inequivalent possible sites with $0.5 < r < 0.55$ nm [corresponding to NNN sites of the second coordination sphere; cf. Fig. 6(a)]. Only these would give detectable contributions to the EPR signal, as shown in the previous section. We considered all five pairs from the first group and a single pair, as an example, from the second group. The results are presented in Table IV.

Both experimental and theoretical results based on calculation with Wannier functions show that there are changes in the *g* tensor components of Ce-Ce pairs with respect to the single

TABLE IV. Principal g tensor components of Ce_1-Ce_2 pair centers for fixed Ce_1 and various locations of Ce_2.

Nearest neighbors (first coordination sphere)					
Substitutional Y(Ce_2) site	**Center**	g_x	g_y	g_z	**Euler angle α**
Y 1	Ce_1	0.0195	0.1272	3.5937	− 27.7
	Ce_2	0.0957	0.1473	3.7643	32.1
Y 2	Ce_1	0.0095	0.0948	3.8244	− 33.5
	Ce_2	0.0267	0.1598	3.5348	26.2
Y 3	Ce_1	0.1353	0.0405	3.8154	− 32.2
	Ce_2	0.1599	0.2465	3.7287	29.7
Y 4	Ce_1	0.0159	0.0402	3.9186	− 33.7
	Ce_2	0.0790	0.1533	3.8453	− 32.7
Y 5	Ce_1	0.1747	0.2272	3.7346	− 34.7
	Ce_2	0.0447	0.0596	3.7222	29.7
Next nearest neighbors (second coordination sphere)					
Substitutional Y(Ce_2) site	**Center**	g_x	g_y	g_z	**Euler angle α**
Y 6	Ce_1	0.1295	0.1756	3.7107	− 31.0
	Ce_2	0.0800	0.1638	3.6794	− 30.1

Ce center. Nevertheless, the absolute value of these changes is small. For the biggest g_z component, which determines the value of the spin-spin interaction, they represent at maximum a few percent. The larger changes are predicted for resonances of pairs with respect to the single ion along the g_x and g_y magnetic axes. But it can hardly be analyzed due to the uncertainty in the resonance fields of pair spectra at low g factors. Note that the DFT calculation shows a bigger difference in the g tensor parameters of two Ce^{3+} ions of a Ce-Ce pair than that obtained from the experiment, obviously due to limited supercell size and overestimated lattice relaxation. Therefore, without knowledge of the exchange energies it is impossible to assign each of the pair centers to an actual position in the lattice.

Using the DFT calculations we also estimated how the dipolar field B_{dip} is influenced by the relaxation of the crystal structure and charge transfer. We selected the NN Ce^{3+} pair in which Ce_1(Ce_2) is located on the Y7 (Y8) site. Taking the Ce magnetic moment as $3.58\,\mu_B$ (the value experimentally determined), the difference of B_{dip} between relaxed and unrelaxed structures amounted to 1.6% and 2.0% for Ce_1 and Ce_2, respectively. To determine the contribution of the oxygen ligands and other ions in the system to B_{dip} we first performed the spin-polarized calculation with the same Ce^{3+} pair and the $4f$ electrons treated as core electrons. In this "open-core" procedure the spins of Ce_1 and Ce_2 were kept parallel; thus the spin moments induced on the ligands were maximized. The magnetic moments on the nearest oxygen ligands ranged from $-0.001\,\mu_B$ to $-0.002\,\mu_B$, the moments on more distant ions being smaller. The contribution of induced moments to B_{dip} was obtained by summation over all ions in a sphere with a radius of 2 nm. The resulting change of B_{dip} was more than two orders of magnitude smaller compared to B_{dip} caused by the Ce^{3+} moments. Therefore, our calculation of the dipole interaction energies by using a simple phenomenological model provides quite realistic values of the dipole interaction energies.

IV. CONCLUSIONS

EPR spectra of single and exchange-coupled Ce^{3+} ions have been studied in $YAlO_3$:Ce crystals. For single Ce^{3+} ions the g tensor principal values were refined. The nearest- and next-nearest-neighbor Ce^{3+} pairs produce satellite lines in the Ce^{3+} EPR spectra. Their resonance fields as a function of magnetic field direction were fitted by a general effective spin Hamiltonian describing two interacting particles with the spin $S = 1/2$ and both the g tensor and spin-spin coupling constants were determined. Calculations show that the magnetic dipolar interaction of the nearest neighbors is about 0.1 and $-0.2\,cm^{-1}$. For the next-nearest neighbors it is in the range–(0.016–0.024) and (0.03–0.05) cm^{-1} depending on both the distance between Ce ions and their position. The exchange interaction between Ce^{3+} ions is essentially anisotropic due to the anisotropy of the g factors. Most probably, it contains both the antisymmetric Dzyaloshinskii-Moriya interaction [34,35] and the symmetric anisotropic exchange caused by strong spin-orbit coupling of Ce^{3+} as well as the low symmetry of the center. The estimated magnitude of the anisotropic exchange is in the range (0.3–0.6) cm^{-1} for both nearest and next-nearest neighbors. It can be even larger for the next-nearest neighbors than for the nearest neighbors, as for Eu^{2+} in the isomorphous $EuTiO_3$ crystal.

We employed a recently developed method of calculation of the crystal field parameters based on transformation from Bloch to Wannier functions to determine the principal g tensor components for both single Ce^{3+} ions and Ce-Ce pairs. The calculated g values provide satisfactory agreement with those determined from EPR spectra. Application of the method to calculate the exchange interaction of Ce-Ce pairs will follow in the near future. Our preliminary attempt in this direction has shown that the task is more demanding than originally thought.

We do not expect the Ce^{3+} pairs to reduce the quantum efficiency of luminescence of YAP:Ce crystals despite the rapid energy transfer between ions coupled by exchange. The reason consists in the lack of $4f$ lower-lying levels of Ce^{3+} which could allow its $5d$ excited state depletion by a cross relaxation or down-conversion process. Such processes, however, should be further studied in Pr^{3+}-doped aluminum perovskites to possibly explain their anomalously low light yield observed in earlier studies [36].

Revealing the Ce^{3+} ion pairing in the YAP host provides an important piece of information which will likely be valid for most of the remaining trivalent rare-earth (R) ions doped into this host. Namely, the pairing of the doped R^{3+} ions with high $4f$ level density will certainly influence the physical mechanisms of other optical phenomena such as lasing, up-conversion, and down-conversion, i.e., phenomena in which the interaction among the doped R ions is critical and which are intensively studied by the large optical community due to their application potential.

ACKNOWLEDGMENTS

The authors gratefully acknowledge the support from the Czech Science Foundation Projects No. P204/12/0805 and No. CZ.2. 13/3.1.00/22132 and the Ministry of Education, Youth and Sports of Czech Republic Projects No. LM2011029 and No. LO1409.

[1] T. Takeda, T. Miyata, F. Muramatsu, and T. Tomiki, J. Electrochem. Soc. **127**, 438 (1980); A. Lempicki, M. H. Randles, D. Wisniewski, M. Balcerzyk, C. Brecher, and A. J. Wojtowicz, IEEE Trans. Nucl. Sci. **42**, 280 (1995).
[2] P. A. Rodnyi, *Physical Processes in Inorganic Scintillators* (CRC Press, New York, 1997).
[3] C. Kuntner, H. Aiginger, E. Auffray, J. Glodo, M. Kapusta, P. Lecoq, M. Moszynski, M. Schneegans, P. Szupryczynski, and A. J. Wojtowicz, Nucl. Instrum. Methods Phys. Res. A **486**, 176 (2002).
[4] M. Nikl, Phys. Status Solidi **178**, 595 (2000).
[5] A. G. Petrosyan, K. L. Ovanesyan, G.O. Shirinyan, T. I. Butaeva, C. Pedrini, C. Dujardin, and A. Belsky, J. Cryst. Growth **211**, 252 (2000).
[6] A. G. Petrosyan, G. O. Shirinyan, K. L. Ovanesyan, C. Pedrini, C. Dujardin, N. Garnier, S. Sowinski, P. Lecoq, and A. Belsky, Nucl. Instrum. Methods Phys. Res. A **486**, 74 (2002).
[7] W. Drozdowski, A. J. Wojtowicz, T. Łukasiewicz, and J. Kisielewski, Nucl. Instrum. Methods Phys. Res. A **562**, 254 (2006).
[8] A. J. Wojtowicz, P. Bruyndonckx, W. Drozdowski, Z. Galazka, J. Glodo, T. Lukasiewicz, P. Szupryczynski, S. Tavernier, M. Wisniewska, and D. Wisniewski, Nucl. Instrum. Methods Phys. Res. A **486**, 482 (2002).
[9] J. Trummer, E. Auffray, P. Lecoq, A. G. Petrosyan, and P. Sempere-Roldan, Nucl. Instrum. Methods Phys. Res. A **551**, 339 (2005).
[10] V. V. Laguta and M. Nikl, Phys. Status Solidi B **250**, 254 (2013).
[11] H. R. Asatryan, J. Rosa and J. A. Mareš, Solid State Commun. **104**, 5 (1997).
[12] H. Asatryan and P. Baranov, Int. J. Mod. Phys.: Conf. Ser. **15**, 16 (2012).
[13] A.Vedda, M. Martini, D. Di Martino, V. V. Laguta, M. Nikl, E. Mihokova, J. Rosa, K. Nejezchleb, and K. Blazek, Radiat. Eff. Defects Solids **157**, 1003 (2002).
[14] V. Laguta, A. Slipenyuk, M. Glinchuk, I. P. Bykov, Yu. Zorenko, M. Nikl, J. Rosa, and K. Nejezchleb, Radiat. Meas. **42**, 835 (2007).
[15] M. Nikl, A. Vedda, M. Fasoli, I. Fontana, V. V. Laguta, E. Mihokova, J. Pejchal, J. Rosa, and K. Nejezchleb, Phys. Rev. B **76**, 195121 (2007).
[16] V. V. Laguta, M. Nikl, A. Vedda, E. Mihokova, J. Rosa, K. Blazek, Phys. Rev. B **80**, 045114 (2009).
[17] V. Babin, L. Grigorjeva, I. Kondakova, T. Kärner, V.V. Laguta, M. Nikl, K. Smits, S. Zazubovich, Yu. Zorenko, J. Phys. D: Appl. Phys. **44**, 315402 (2011).
[18] M. Buryi, V. Laguta, J. Rosa, M. Nikl, Adv. Sci. Eng. Med. **7**, 258 (2015).
[19] P. Novák, K. Knížek, J. Kuneš, Phys. Rev. B **87**, 205139 (2013).
[20] S. Geller and E. A. Wood, Acta Crystallogr. **9**, 563 (1956).
[21] R. D. Shannon, Acta Crystallogr. Sect. A: Cryst. Phys., Diffr., Theor. Gen. Crystallogr. **32**, 751 (1976).
[22] A. Abragam and B. Bleaney, *Electron Paramagnetic Resonance of Transition Ions* (Clarendon Press, Oxford, 1970).
[23] S. Geschwind, *Electron Paramagnetic Resonance* (Plenum Press, New York, 1972).
[24] R. J. Birgeneau, M. T. Hutchings, and R. N. Rogers, Phys. Rev. **175**, 1116 (1968).
[25] T. R. McGuire, M. W. Shafer, and R. J. Joenk, J. Appl. Phys. **37**, 981 (1966).
[26] P. Novák, J. Kuneš, and K. Knížek, Opt. Mater. **37**, 414 (2014).
[27] E. Mihóková, P. Novák, and V. V. Laguta, (unpublished).
[28] P. Novák, K. Knížek, M. Maryško, Z. Jirák, and J. Kuneš, J. Phys.: Condens. Matter **25**, 446001 (2013).
[29] P. Novák, V. Nekvasil, and K. Knížek, J. Magn. Magn. Mater. **358–359**, 228 (2014).
[30] P. Blaha, K. Schwarz, G. K. H. Madsen, D. Kvasnicka, and J. Luitz, computer code WIEN2K, *An Augmented Plane Wave + Local Orbitals Program for Calculating Crystal Properties* (Technische Universität, Wien, Austria, 2001).
[31] B. G. Wybourne, *Spectroscopic properties of rare earths* (Interscience, New York, 1965).
[32] M. J. Weber, J. Appl. Phys. **44**, 3205 (1973).
[33] S. Kammoun and M. Kamoun, Phys. Status Solidi B **229**, 1321 (2002).
[34] I. Dzyaloshinsky, Phys. Chem. Solids **4**, 241 (1958).
[35] T. Moriya, Phys. Rev. **120**, 91 (1960).
[36] M. Nikl, J. A. Mares, A. Vedda, M. Fasoli, V. Laguta, E. Mihokova, J. Pejchal, M. Zhuravleva, A. Yoshikawa, and K. Nejezchleb, IEEE Trans. Nucl. Sci. **57**, 1168 (2010).